

Influence of Pavement Edge and Shoulder Characteristics on Vehicle Handling and Stability

DON L. IVEY and DEAN L. SICKING

ABSTRACT

Described in this paper is an analytical approach to predicting the steer angle of a vehicle, which is necessary to mount a pavement edge from the scrubbing condition. This steer angle is dependent on a new concept, the effective edge height, pavement edge geometry, travel lane friction and shoulder friction, tire geometry, and tire-cornering characteristics. It is demonstrated how this steer angle prediction can be combined with a vehicle simulation such as highway vehicle object simulation model (HVOSM) to predict vehicle movements, stability, and controllability. It is concluded that this combination of analyses used with driver performance characteristics now allows the study of a variety of factors. These would include all vehicle characteristics defined by HVOSM and many highway properties. Principal among these highway properties are pavement, shoulder and edge surface friction, and edge height and shape.

The possibility of a driver losing control after the vehicle goes off the paved surface onto a shoulder has caused highway engineers great concern. Why this occurs and under what conditions it can occur has been the subject of research efforts by Klein et al. (1), Nordlin and Stoughton (2,3), and Zimmer and Ivey (4). These efforts have been summarized in TRB State-of-the-Art Report 1, "The Influence of Roadway Surface Discontinuities on Safety" (5). Recently Graham and Glennon have tried to use computer simulation to study the phenomenon of vehicle loss of control due to pavement edges (6). In all these efforts no one has tested a large group of drivers. This is a recognized shortcoming, but the necessary resources were simply not available. To alleviate this problem, the Transportation Research Board is sponsoring a new study at the University of Michigan Transportation Research Institute and Texas Transportation Institute. Testing of a wide spectrum of drivers in highway environments is being conducted to better define driver performance. This work includes edges of different sizes and shapes. Still, there will not be enough funding to test all edge conditions of interest.

The work presented here is an effort to provide an analytical approach to the evaluation of a variety of edge conditions using the most reliable vehicle handling simulation--that venerable code developed by McHenry et al.--highway vehicle object simulation model (HVOSM) (7). The difficulty in using HVOSM directly has been in simulating tire edge interaction with reasonable accuracy. In this paper that difficulty is overcome by the development of an analysis that predicts the steer angle necessary to mount a specific edge from the scrubbing (4) condition. Once that value is determined as a function of edge height, edge shape, tire size, tire-pavement cornering characteristics, and other physical parameters, it can be used as one input parameter to HVOSM to define initial conditions. HVOSM, in an unmodified

form, will then define vehicle response as a function of vehicle and driver performance characteristics. Presented in this paper in abbreviated form is the analytical development to predict initial steer angle, and the use of HVOSM is demonstrated to determine subsequent vehicle response. The results are most encouraging. This technique can be used to extrapolate driver performance characteristics now being observed in the TRB study to a variety of physical situations and to define parametrically the influence of specific factors on vehicle handling and stability.

ABBREVIATED THEORETICAL DEVELOPMENT

Consider an automobile with one set of wheels off the pavement edge but with the inside of those wheels brushing that edge as shown in Figure 1. As the driver turns the steering wheel in an effort to mount the edge to return to the paved surface, the steering angle of the front wheels, α , is gradually increased. As α gets larger, the vehicle will finally climb the edge when the right front wheel reaches the critical value of α , α_c . Further, the right rear tire will finally mount the edge when the yaw of the vehicle has increased to approximately α_c . The vehicle speed, yaw, and yaw rate at this predictable vehicle position, along with the driver's reaction time and counter steering capability will then dictate whether the vehicle can be successfully controlled. The critical steer angle, α_c , is therefore of major importance in predicting vehicle controllability. This abbreviated derivation is an attempt to predict that critical steer angle. The complete derivation is available on request from the authors.

FORCES ACTING ON THE FRONT TIRES

As a vehicle in the edge scrubbing condition has its wheels gradually turned into the pavement edge surface, a state of equilibrium exists between the

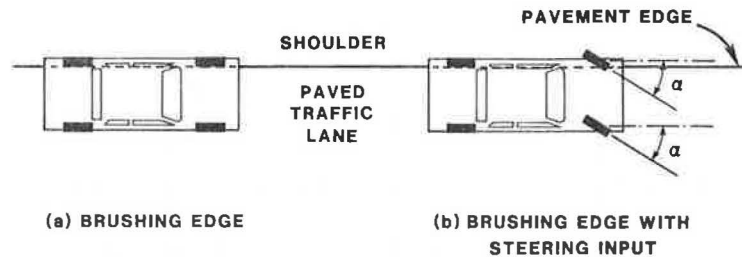


FIGURE 1 Vehicle gradually turning toward a pavement edge.

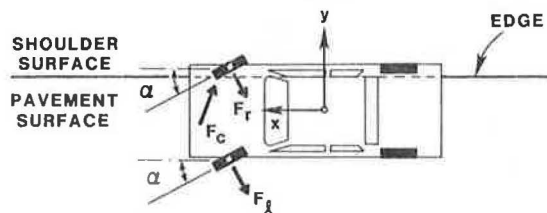


FIGURE 2 Equilibrium of forces acting on vehicle front tires.

cornering forces on the two front wheels and the resisting force generated by the edge, as shown in Figure 2.

A summation of the forces acting on the front tires in the y direction yields

$$\vec{F}_r + \vec{F}_l = \vec{F}_c \quad (1)$$

where F_r is the cornering force exerted on the right front tire, F_l is the cornering force exerted on the left front tire, and F_c is the force exerted by the pavement edge on the right front tire.

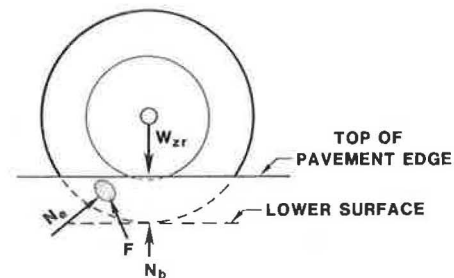
The cornering forces can be determined by knowledge of the lateral force generation characteristics of the tires in contact with specific surfaces, the vertical load at the pavement or shoulder surface on each front tire, and the slip angle, α , of each front tire.

The definition of the magnitude and direction of the edge force, F_c , is somewhat more difficult. First, it will be assumed that the edge force, F_c , is the resultant of two forces. These are N_e , a force acting normal to the undeformed surface of the tire at the center of the area of tire-edge contact, and F , the friction force acting at the tire and edge contact zone. This friction force must act in opposition to the relative velocity between the tire and edge surface and in the plane of the contact zone, assuming further that plane is defined by the undeformed surface of the tire. These forces are shown in Figure 3. A summation of forces vertically yields

$$\vec{N}_b + \vec{N}_e + \vec{F} = \vec{W}_{zr} \quad (2)$$

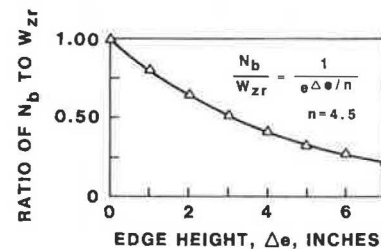
The normal force, N_b , acting on the bottom contact patch of the tire is difficult to deal with analytically. At some point, this force obviously becomes zero for the larger edge heights as mounting starts. This variation of N_b with edge height was assumed to vary as shown in Figure 4. An n value of 4.5 was tentatively selected to give an appropriate fit of test data. This will be discussed further in the final section. Using this approximation for N_b , Equation 2 can be written

$$\vec{W}_{zr}/e^{\Delta e/n} + \vec{N}_e + \vec{F} = \vec{W}_{zr}$$



W_{zr} = the weight of and on the right front wheel,
 N_b = the normal force on the bottom contact path,
 N_e = the normal force acting at the contact zone of the tire with the pavement edge, and
 F = the friction force acting on the tire-edge contact zone.

FIGURE 3 Forces on the tire in contact with the pavement edge.

FIGURE 4 Reduction of N_b as the effective edge height increases.

In the full derivation it has been shown that Equations 1 and 2 can be expressed in terms of the geometric characteristics of the tire and the pavement edge and two unknowns N_e and α_c . With these equations, N_e can be eliminated and the slip angle, α_c , necessary to climb a specific pavement edge, may be calculated.

EFFECTIVE EDGE HEIGHT

It is intuitively appealing that more gradually sloped edges are easier for a tire to mount than sharp, abrupt edges, just as it is easier to walk up a gradual incline than to climb a cliff. If it is noted how a tire makes contact with edges of different shapes, as shown by Figure 5, it becomes apparent that the relative ease or difficulty a tire encounters in traversing a particular edge may be explained by the idea of effective edge height. The effective edge height is defined as the height above the lower surface (usually considered the shoulder surface) at which the tire makes predominant contact with the edge. In earlier discussions this has been called the contact zone, and is defined as the area at which the normal force, N_e , and the friction force, F , act. As observed in Figure 5, a right-angle

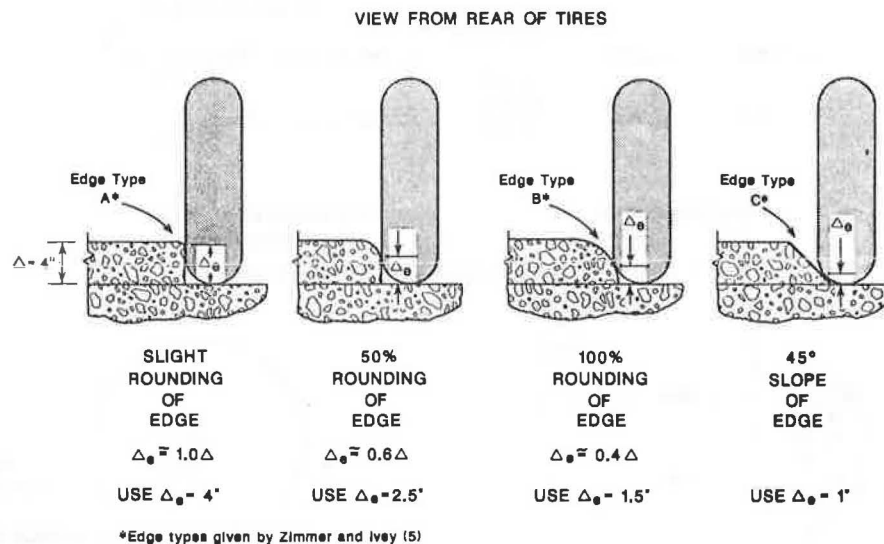


FIGURE 5 Effective edge heights for different edge shapes.

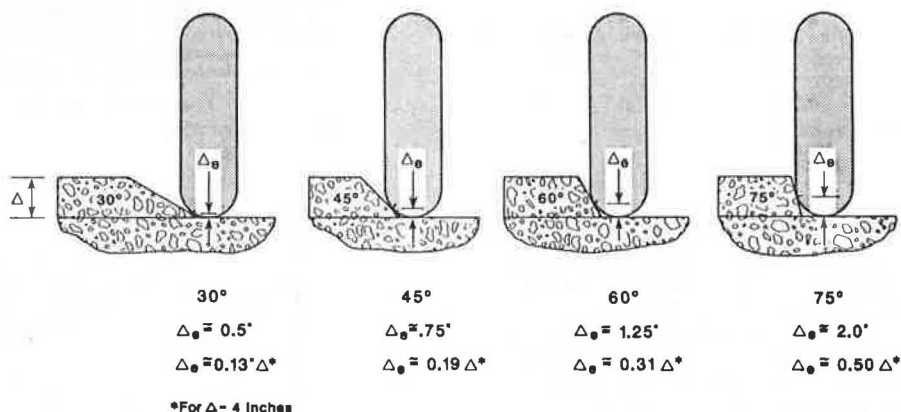


FIGURE 6 Effective edge heights for different edge slopes.

edge has an effective height, Δ_e , roughly equivalent to the total vertical distance, Δ , between the two major plane surfaces (i.e., the pavement surface and the shoulder surface). As different edge shapes are considered, it is apparent that the effective height becomes smaller as the edge becomes more rounded, and finally sloped at an angle of 45 degrees. Both empirical testing and the theory presented here, demonstrate conclusively the greater ease of traversing more rounded and more gradually sloped edges (1-4).

Figure 6 shows the influence of different edge slope angles on the effective height, and Figure 7 shows the complete variation from an edge slope of zero degrees, which must certainly correspond to a zero effective height, to a slope of 90 degrees, which is just as certainly an effective height, Δ_e , equal to the total height, Δ .

A range of angles probably exists between 60 and 90 degrees where the concept of effective height less than the total height breaks down. This is due to tire deformation producing tire surface compliance with edge geometry and the simplified geometry attributed to the tire cross section in this development.

The effective height is only slightly influenced by the steer or slip angle, α , in the range of importance, from 0 to 15 degrees. This small variation may be considered of only academic interest.

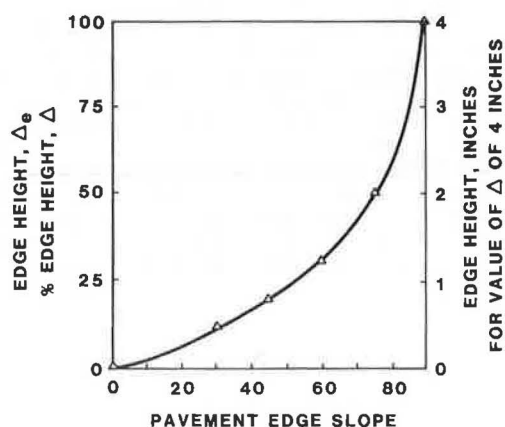


FIGURE 7 Effective edge height variation with edge slope.

It appears compelling then that the concept of effective height explains in simple geometric terms the resistance a tire (or vehicle) encounters in traversing edges of the same total height but of quite different shape. In subsequent sections, the concept of effective height will be used, along with

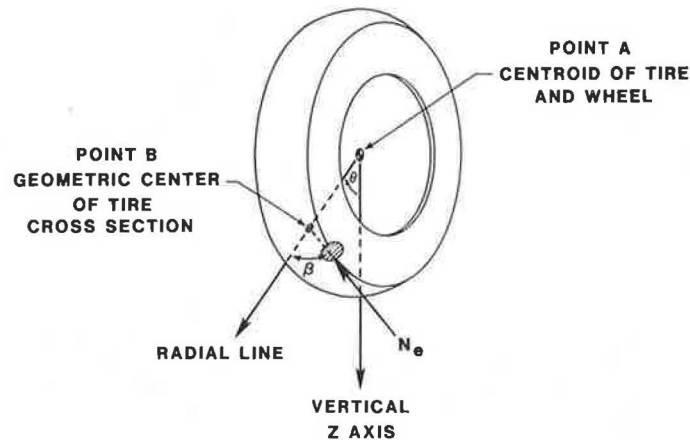


FIGURE 8 Perspective of tire.

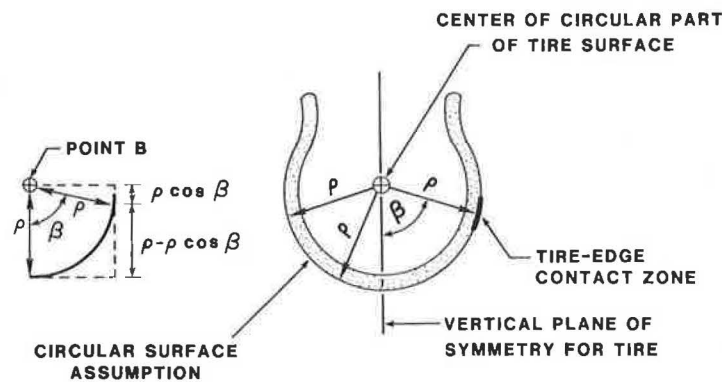


FIGURE 9 Cross section of tire.

the theoretical analysis to calculate those resistances.

NORMAL FORCE

Figure 8 is a perspective view of the tire and wheel showing the direction of the normal force, N_e , that is developed between the tire and the edge. The normal force is assumed to act in a direction normal to the undeformed surface of the tire. A further simplification is that the surface of the tire cross section is circular and is defined by a radius, ρ , about point B (see Figure 9). Although it is recognized that tires are not circular in cross section, the authors believed that the circular simplification would not seriously compromise accuracy. The results appear to bear this out.

The following geometric measurements were used to resolve the normal force into transverse and vertical components.

θ , the angle between the vertical plane, including the wheel axis and a second plane defined by the wheel axis and the tire-edge contact zone.

r , the radial distance from the wheel axis to the contact zone.

r_t , the undeformed tire radius.

r_r , rolling radius of the tire (note this can be approximated by r_t when the tire starts to mount the pavement edge).

Δ_e , the effective height of the pavement edge (i.e., the height of the tire-edge contact zone above the lower surface).

ρ , the approximate radius of curvature of the tire cross section as shown in Figure 9.

β , the angle in the plane of the tire cross section between the central plane cross section and the edge contact zone. (See Figures 8 and 9.)

The transverse component of $N_e \sin \theta$ is found to be $N_e \sin \beta$ and the vertical component of N_e is $N_e \cos \beta \cos \theta$.

FRICTION FORCE

Now the friction force, F , acting in the tire-pavement edge contact zone will be considered. Figure 10 is a side view of the tire-edge contact patch showing the velocity components V_l and $\dot{\theta}_r$ and the resultant velocity V_r . These geometric and dynamic parameters may be used to define the transverse and vertical components of the force F . Thus the transverse com-

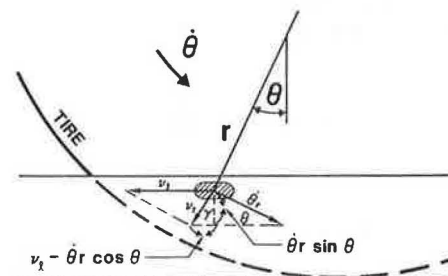


FIGURE 10 Relative velocity between tire and pavement edge.

ponent of F is $F \cos \gamma \cos \beta$ and the vertical component of F is $F \cos \gamma \sin \beta$.

DETERMINATION OF TIRE-CORNERING FORCE

In determining the conditions under which a tire will mount an edge, it is necessary to estimate the tire-cornering force when the slip angle, α , is equal to the critical slip angle, α_c . This is done by calculating the slope of a line between zero slip angle and points on the side force, slip angle curve. Figure 11 shows how this is done. If these slopes C'_α are estimated from the side force, slip angle curve for a particular tire, surface, and tire load, a curve relating C'_α to α can be plotted in Figure 12. By dividing all values of C'_α by the load at which the test was conducted, C'_α can be made dimensionless and the two lines, A and B, can be expressed.

$$C_\alpha = K_1 - K_2\alpha, 0 < \alpha \leq \alpha_d \quad (\text{Line A})$$

$$C_\alpha = K_3 - K_4\alpha, \alpha > \alpha_d \quad (\text{Line B})$$

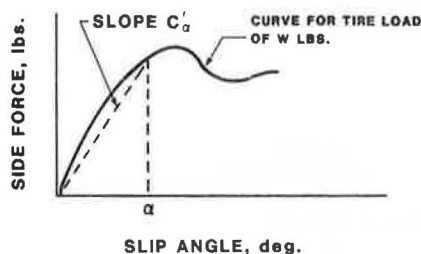
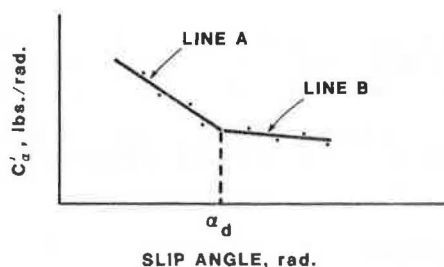


FIGURE 11 Side force, slip angle curve.



$$C_\alpha = K_1 - K_2\alpha, 0 < \alpha \leq \alpha_d \quad (\text{LINE A})$$

$$C_\alpha = K_3 - K_4\alpha, \alpha > \alpha_d \quad (\text{LINE B})$$

FIGURE 12 Slope-slip angle and straight-line approximation.

Sakai used Figure 26 in "Characteristics of Japanese ESV Tires" (8) to calculate values for K_1 through K_4 . For a 6.45-14-4PR (5J-14 rim) conventional tire, the K values calculated were

$$\begin{aligned} K_1 &= 8.04 \\ K_2 &= 17.1 \\ K_3 &= 8.04 \\ K_4 &= 17.1 \end{aligned} \quad \begin{array}{l} \text{One line was sufficient to adequately} \\ \text{describe the data.} \end{array}$$

EQUILIBRIUM EQUATIONS

In reading the equations in this section the reader will see that static equations have been used and the inertial terms needed to define the dynamic

equilibrium of an accelerating body have been neglected. It was believed that this would not compromise accuracy for the following reason. In the instant before edge mounting begins, a vehicle in an edge scrubbing condition at a constant speed does not have significant accelerations imposed on any element. This obviously neglects the random accelerations caused by surface roughness. The authors have a philosophy of problem solving that does not respect sophistication for its aesthetic properties. It is thus submitted that the static treatment is adequate for the purposes of this analysis.

With the resolution of the normal and friction forces acting on the pavement edge, it is now feasible to write Equations 1 and 2 in different terms.

First considering Equation 1 and noting that the cornering force on each wheel can be represented by

$$W_z C_\alpha \alpha$$

where W_z is the weight on a particular wheel contact patch and C_α is the unit cornering stiffness at a slip angle α , Equation 1 can be written

$$W_{zr} S C_{\alpha_c} + W_{zl} C_{\alpha_c} \alpha_c = N_e \sin \beta \cos \alpha_c + F \cos \gamma \cos \beta \cos \alpha_c \quad (3)$$

If the coefficient of friction between the pavement edge and the tire is μ_e , F can be replaced by $\mu_e N_e$. S is the reduction of C_{α_c} due to lower shoulder friction, and the term $e\Delta e/n$ produces a reduction in N_b as the effective edge height, Δe , becomes larger. Note that n is an empirically determined constant. This equation can be rewritten

$$\begin{aligned} (W_{zr}/e\Delta e/n) S C_{\alpha_c} \alpha_c + W_{zl} C_{\alpha_c} \alpha_c = \\ N_e \sin \beta \cos \alpha_c + \mu_e N_e \cos \gamma \beta \cos \alpha_c \end{aligned} \quad (4)$$

Equation 2 can also be rewritten

$$\begin{aligned} N_e \cos \beta \cos \theta + \mu_e N_e \cos \gamma \sin \beta = \\ W_{zr} - W_{zr}/e\Delta e/n \end{aligned} \quad (5)$$

By solving Equation 5 for N_e and substituting that value into Equation 4, the result is one equation with one unknown, α_c . The value of α_c may be calculated by successive approximation.

For a BR 60SR14 (6Jx14 rim) the K values calculated were

$$\begin{aligned} K_1 &= 15.6 \\ K_2 &= 74.0 \\ K_3 &= 8.04 \\ K_4 &= 17.1 \end{aligned} \quad \begin{array}{l} \text{Line A coefficients} \\ \text{Line B coefficients} \end{array}$$

If C_α calculated in this way is multiplied by the weight supported by the tire and the slip angle in radians, the result is the cornering force for the value of α used in either the Line A or Line B equations. If the critical value of slip angle, α_c , is used, the cornering force on the non-mounting front tire may be calculated.

COMPARISON WITH EMPIRICAL OBSERVATIONS

Independent observations of the steer angle necessary to climb a pavement edge from the scrubbing condition were provided in a 1976 paper by Klein et al. (1). They made observations on four vehicles shown in the

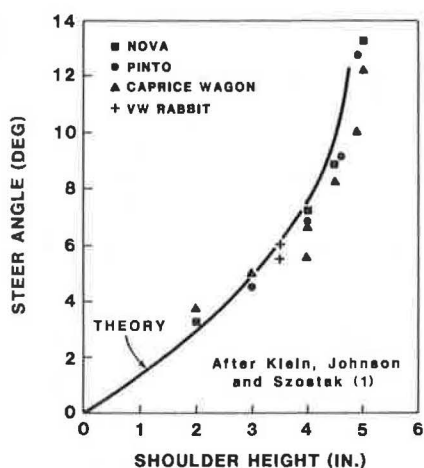


FIGURE 13 Steer angle required to climb various edge heights from a scrubbing condition for four cars compared with theoretical predictions.

legend of Figure 13 and came to the conclusion that the steer angle was somewhat independent of vehicle and tire size, at least within the range tested and testing accuracy.

To compare the theory with the empirical observations shown in Figure 13, the following parameters were used: A nominal 14-in. tire, roughly comparable to the "conventional tire" given by Sakai (8). (See Figure 14.) The tire radius, r_t , was taken at 12.5 in.; the rolling radius r_r , at 12.0 in.; the tire cross-section radius, ρ at 3.6 in.; and nominal values of K_1 , K_2 , K_3 , and K_4 were 9, 18, 9, and 18, respectively. These values are very close to those derived from the conventional tire side force, slip angle data, although the surface in the Sakai (8) tests was different from that in Klein et al. (1). The tire-edge friction coefficient, μ_e , was 0.7; the shoulder-friction reduction factor, S , was 0.8; and n the vertical force, N_b , reduction factor was 4.5.

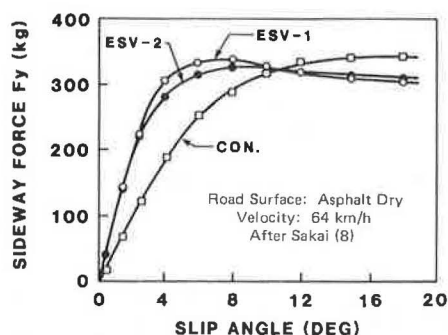


FIGURE 14 Side force-slip angle curves for three tires.

Based on these estimates, the theory curve shown in Figure 13 was generated. Although these results appear to be excellent because the factors used appear to be reasonable estimates of the conditions of the tests, it must be recognized that the factor, n , the vertical force reduction factor was selected to give an appropriate fit of the data. Figure 15 shows that the relationship produced by the theory is heavily dependent on the value of n selected. That is, the slip angle predicted to climb a specific

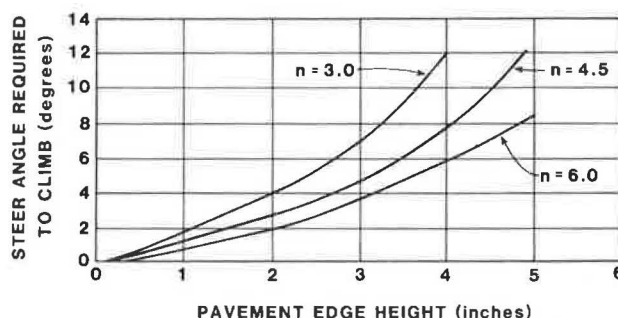


FIGURE 15 Influence of N_b reduction factor.

edge is heavily dependent on the amount of the weight borne by the tire-shoulder surface contact zone at the time mounting occurs.

In order to objectively assess the predictive accuracy of the theory, it would be necessary to experimentally determine the following factors: (a) μ_e , (b) S , (c) n , and (d) k_1 through K_4 .

The appropriate equations developed in this study were programmed for solution and for graphics display by Robert Streckfus. The program listing is available to any interested party. The results of Streckfus' study of the influence of several different parameters is shown in Figures 16 through 19.

In Figure 16, the curves from left to right above the 6-degree steering angle line are for values of the pavement edge friction of 0.3, 0.7, and 0.9, respectively.

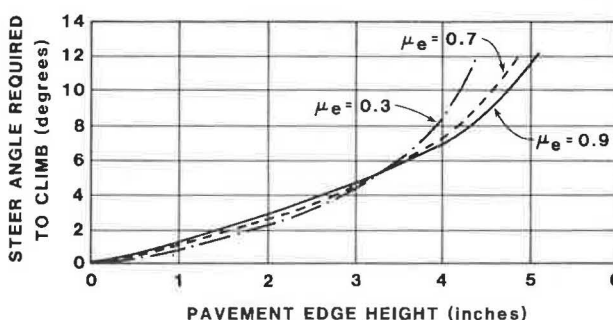


FIGURE 16 Influence of pavement edge friction.

Figure 17 shows the influence of the shoulder friction reduction factor as it varies from 0.1 to 1.0. An icy shoulder might be represented by an S factor as low as 0.1. If the pavement friction is 0.7, the icy shoulder friction would be 0.1 times 0.7 or 0.07. That situation would be more critical.

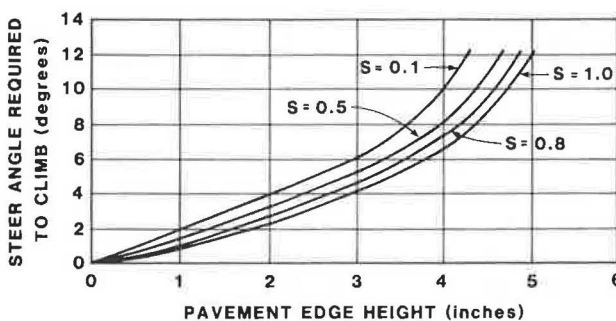


FIGURE 17 Influence of shoulder friction reduction factor.

than the shoulder conditions under which more friction could be developed. It is surprising that it is not more influential until it is considered that only a portion of the wheel weight, N_D , is active on the shoulder surface when mounting occurs. By saying a shoulder has little effect on the steer angle to mount, it does not follow that the influence on vehicle loss of control is also small. The contrary is actually true.

Figure 15 shows that the value of N_D , and the rate it is reduced, as dictated by the factor n , is most important. From left to right, the orange curves are shown using n values of 3.0, 4.5, and 6.0, respectively. The value of 4.5 was believed to give the most appropriate, albeit slightly conservative, representation of the data developed by Klein et al. (1).

Figures 18 and 19 show how the tire-cornering force coefficients influence the solution. Larger K_1 and K_3 values give higher values of cornering force. These curves, from left to right in Figure 18, show the sensitivity of the theory as K_1 and K_3 vary from 7 to 11. Smaller values of K_2 and K_4 give larger values of tire-cornering force. Figure 19 shows the influence from left to right of values of K_2 and K_4 of 21, 18, and 15, respectively.

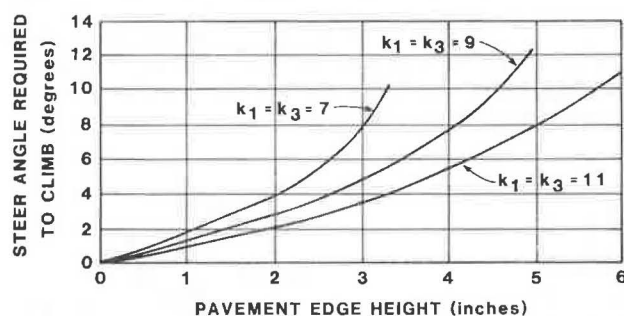


FIGURE 18 Influence of tire-cornering force coefficient.

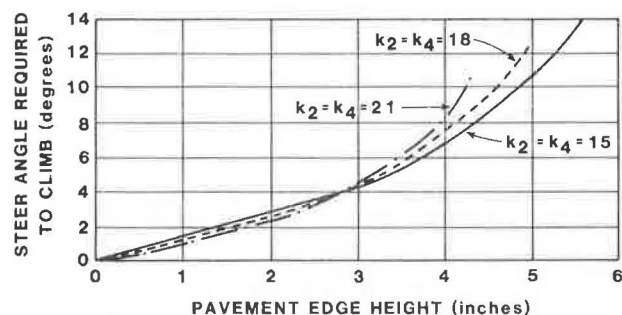


FIGURE 19 Influence of tire-cornering force coefficient.

The base reference values of the five coefficients for these sensitivity studies are

$$\begin{aligned} \mu_e &= 0.7 \\ s &= 0.8 \\ n &= 4.5 \\ K_1 &= K_3 = 9.0 \\ K_2 &= K_4 = 18.0 \end{aligned}$$

These are the same values used to produce the comparison between theory and test data shown in Figure 13.

These results show a high probability that the theory developed here can provide meaningful predic-

tions of the tire-cornering slip angles necessary to mount defined pavement edges. It is a relatively easy step to move from this prediction to the assessment of safety for various edge conditions. Models such as the relatively simple one given by Klein et al. (1), or HVOSM (7), can be used to estimate automobile response subsequent to mounting a pavement edge at a specific condition of cornering slip angle. In the final section, HVOSM will be used to demonstrate how driver and vehicle performance can be assessed by using this combination of analyses.

VEHICLE MOVEMENT SUBSEQUENT TO EDGE MOUNTING

To demonstrate how the foregoing development can be used to study vehicle movements HVOSM was used. This code was selected as the most comprehensive and reliable of the codes available. It was developed by McHenry et al. (7) in the late 1960s, and has been widely used in the highway safety field since that time.

The vehicle selected for this demonstration was a 1974 Chevrolet Luv Pickup. The data used to simulate that vehicle and the various maneuver conditions are available but are not presented here. Nine edge conditions were selected and are given in Table 1, along with the value of critical steer angle, α_c , used as an initial condition.

Conditions 1, 2, and 3, were selected to show the effect of progressive degrees of rounding on vehicle responses after an edge climb. In order to determine vehicle response, an additional set of input parameters was required.

1. Initial steer angle. This was determined as follows: First an effective edge height was determined using the methods described previously. For example, the effective edge height for Conditions 1, 2, and 3, can be taken from Figure 5. They are 4.0, 2.5, 1.5, and 1.0 in. (Actually 0.75 in. was used instead of 1.0, as showing the more accurate value from Figure 8.) The values of Δ_e , effective edge height, were taken from Figure 7 for Conditions 4 through 9.

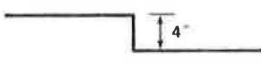


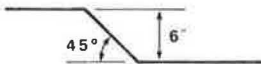

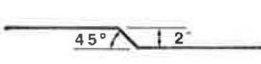
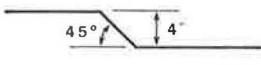
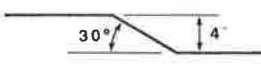
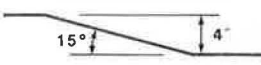
2. Using the value of Δ_e defined, the steer angle was determined using Figure 13. These values of steer angle are given in the final column of Table 1.

3. Driver control characteristics were required for each test run. On the basis of data developed by Zimmer and Ivey (4) and new data from the ongoing UMTRI/TTI study, values of a combined perception reaction time and a front wheel turning speed were selected. Approximate mid-range values of these performance characteristics were 0.5 sec and 16 degrees per sec. That is, the driver would start moving the steering wheel 0.5 sec after the right front tire mounted the edge from a scrubbing condition, and the rate of wheel movement would be 16 degrees per sec.

4. With these values of initial steer angle and driver control characteristics, the nine program runs given in Table 1 were produced.

Example output data selected from Condition 1 are given in Table 2. The initial speed on all runs was 50 mph (73.33 fps). The time elapsed after edge mounting begins is given in the first column. The position of the vehicle's center of gravity (c.g.) is given in the next three columns (x' = forward, y' = lateral, and z' = down). The sprung mass rotational orientation is given by the next three columns (Φ = roll, Θ = pitch, and Ψ = yaw). The lateral, vertical, and forward speeds are given in the last three columns. The resultant velocity of the vehicle is the vector sum of these three velocities.

TABLE 1 Pavement Edge, Effective Edge Heights, and Initial Steer

Condition	Pavement Edge Profile	Effective Edge Height, Δ_e , inches	Initial Steer Angle, α_c , degrees
1		4.0 (From Figure 5)	7.5 ^a
2		2.5 (From Figure 5)	3.8 ^a
3		1.5 (From Figure 5)	2.1 ^a
4		0.75 (From Figure 7)	1.1 ^a
5		0.75 (From Figure 7)	1.1 ^a
6		0.75 (From Figure 7)	1.1 ^a
7		0.75 (From Figure 7)	1.1 ^a
8		0.50 (From Figure 7)	0.7 ^a
9		0.20 (From Figure 7)	0.5 ^a

^aThese values determined from the effective edge height and Figure 15.

TABLE 2 Selected Computer Program Results (Condition 1)

Time (sec)	Position (in.)			Sprung Mass c.g. Orientation (deg)			Velocity (fps)		Forward Speed (fps)
	X'	Y'	Z'	Phi	Theta	Psi	Lateral	Vertical	
.0000	500.00	1,174.44	-25.71	4.93	.00	.00	.00	.00	73.33
.5500	980.34	1,171.78	-26.78	2.3	0.91	-1.71	1.20	0.76	72.15
1.1000	1,450.99	1,147.37	-27.16	6.35	-0.31	-18.63	14.10	-1.96	68.71
1.725	1,941.65	1,032.10	-27.45	6.66	-0.10	-49.78	31.96	-3.79	55.30
2.2750	2,301.60	864.80	-27.51	6.65	-0.07	-76.27	40.06	-4.69	39.11
2.5000	2,425.33	786.10	-27.54	6.58	0.00	-86.87	41.20	-4.76	32.02

Using these data from each condition run, Figures 20-22 were plotted. The only values needed to make these figures were X' and Y', movements of the c.g., and the yaw angle.

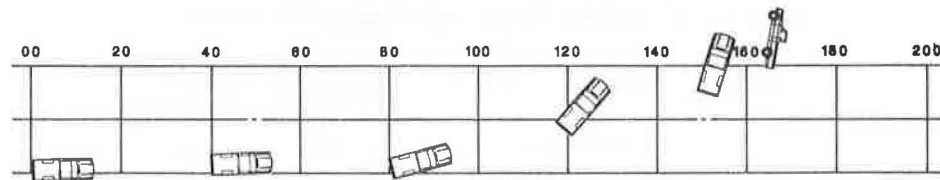
Figure 20 shows the influence of edge rounding. A sharp edge (Condition 1) 4 in. high throws the vehicle completely out of control. Progressive rounding (Conditions 2 and 3) rapidly reduces the problem. Some license has been taken with the vehicle plots of Condition 1. The final view of the vehicle on its side was not predicted by HVOSM. This was done to illustrate that a vehicle in an 86-degree lateral drift certainly has the potential of rolling.

Figure 21 shows the influence of edge height for a 45-degree sloped edge. Although the 6-in. edge (Condition 4) allows the vehicle to barely remain within its lane, the 4- and 2-in. edge allow progressively greater margins of safety. The primary

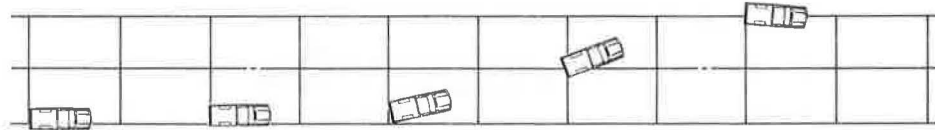
difference in vehicle control in these three runs stemmed from the fact that the 0.5 sec perception-reaction time was not programmed to begin until the right front tire had reached the top of the 45-degree surface. This is probably a conservative assumption; that is, many drivers would begin their perception before fully mounting the edge.

The influence of edge slope is shown in Figure 22. As the slope is reduced from 45 to 15 degrees, the margin of safety, as illustrated by how much of a 12-ft lane is needed for the maneuver, becomes progressively larger.

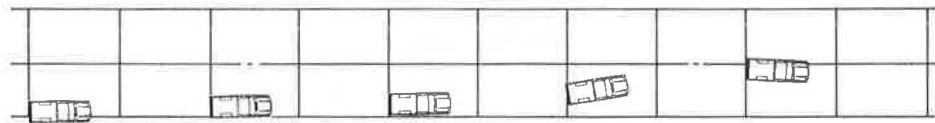
When elements of Figures 20-22 are compared with driver and vehicle performance given in the literature (1-4), and with testing from the ongoing UMTRI/TTI project, good agreement is noted with the mid-range of driver performance. It is therefore submitted that the combination of the analytical pre-



Condition 1 4 inch edge, no rounding
(Predicted steer angle, 7.5 degrees)

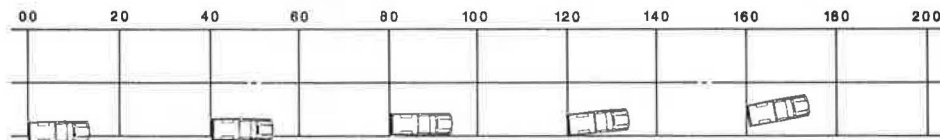


Condition 2 4 inch edge, 2 inch radius of edge rounding
(Predicted steer angle, 3.8 degrees)

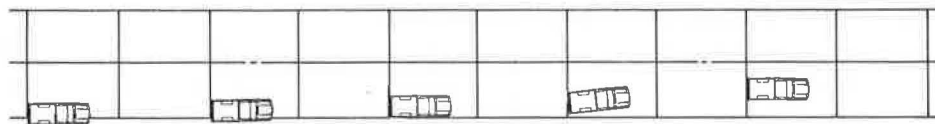


Condition 3 4 inch edge, 4 inch radius of edge rounding
(Predicted steer angle, 2.1 degrees)

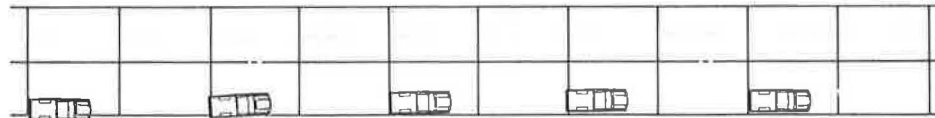
FIGURE 20 Conditions 1, 2, and 3.



Condition 4 6 inch edge, 45 degree edge slope
(Predicted steer angle, 1.1 degrees)



Condition 5 4 inch edge, 45 degree edge slope
(Predicted steer angle, 1.1 degrees)



Condition 6 2 inch edge, 45 degree edge slope
(Predicted steer angle, 1.1 degrees)

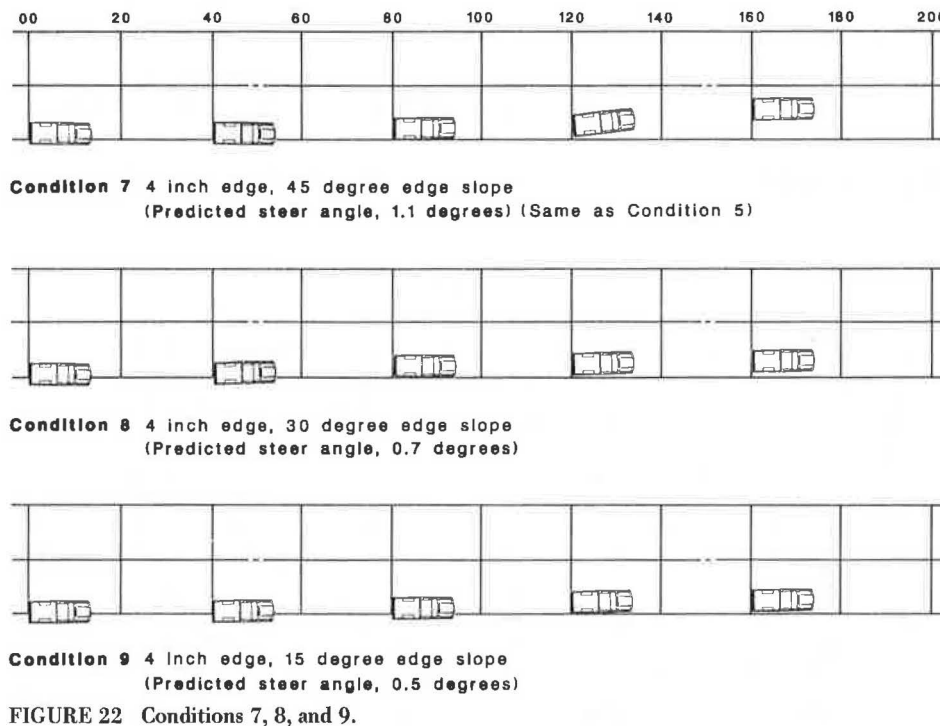
FIGURE 21 Conditions 4, 5, and 6.

diction of initial steering angle and HVOSM has the potential of extrapolating the economically limited full-scale testing programs to analytically estimate the influence of such factors as

1. Vehicle characteristics
 - a. Geometry
 - b. Inertial properties
 - c. Tire geometry
 - d. Tire-surface cornering force characteristics

2. Highway properties
 - a. Pavement surface characteristics (friction development potential)
 - b. Shoulder surface characteristics
 - c. Edge height and shape
 - d. Edge surface characteristics

Based on the driver performance characteristics now being determined, these analyses can be conducted using as broad a spectrum of driver performance as is reasonable. With this combination, continually



checking for agreement with full-scale testing, the full spectrum of highway conditions can be studied and specific situations may be evaluated.

ACKNOWLEDGMENTS

This paper is dedicated to A.D. Ivey, the best intuitive mechanical and civil engineer I have known. It is his "feeling" for physical mechanisms and structures that has helped me simplify and solve many engineering problems, including this one.

DLI

REFERENCES

1. R.H. Klein, W.A. Johnson, and H.T. Szostak. Influence of Roadway Disturbances on Vehicle Handling. DOT HS-802 210. U.S. Department of Transportation, 1976.
2. E.F. Nordlin et al. The Effect of Longitudinal Edge of Paved Surface Drop-Off on Vehicle Stability. CALTRANS Report CA-DOT-TL-6783-1-76-22. Sacramento, Calif., March 1976.
3. R.L. Stoughton et al. The Effect of a Broken A.C. Pavement Drop-Off Edge and Muddy Shoulder on Vehicle Stability and Controllability. CALTRANS Memorandum Report, Sacramento, Calif., July 1978.
4. R.A. Zimmer and D.L. Ivey. Pavement Edges and Vehicle Stability--A Basis for Maintenance Guidelines. Presented at 61st Annual Meeting of the Transportation Research Board, Washington, D.C., Jan. 1983.
5. D.L. Ivey et al. The Influence of Roadway Surface Discontinuities on Safety. State of the Art Report 1, TRB, National Research Council, Washington, D.C., 1984, 45 pp.
6. J.L. Graham and J.L. Glennon. Work Zone Design Considerations for Truck Operations and Pavement/Shoulder Drop-Offs. Midwest Research Institute, Report 7020-S. Kansas City, Mo., Feb. 1984.
7. R.C. McHenry, D.J. Segal, and N.J. DeLays. Determination of Physical Criteria for Roadside Energy Conversion Systems. Cornell Aeronautical Laboratory, Cornell University, Buffalo, N.Y., July 1967.
8. H. Sakai. Characteristics of Japanese ESV Tires. Japan Automobile Research Institute, Inc. Fifth International Conference on Experimental Safety Vehicles, London, England, 1974.

Publication of this paper sponsored by Committee on Surface Properties--Vehicle Interaction.